Accurate Analysis of Arbitrarily Shaped Patch Resonators on Thin Substrates

THOMAS M. MARTINSON AND EDWARD F. KUESTER, MEMBER, IEEE

Abstract — Based on a generalized edge boundary condition (GEBC), an accurate analysis method for arbitrarily shaped microstrip patch resonators is developed. The edge of the patch and its feeding line are first discretized as a series of connected segments. Next, an equivalent voltage and an equivalent current are defined on each segment. This boundary of the patch and the feeding line can be viewed as an interface between two networks. The first takes into account the coupling under the patch. The second represents the dynamical edge effects and the coupling over the top side of the patch. This general and computer-efficient approach is then successfully applied to determine the input impedance of some commonly used probe-fed and strip-fed patch resonators.

I. Introduction

ALTHOUGH MICROSTRIP patch resonators have been studied extensively only in the last decade, many different approaches have been proposed. We can distinguish two general ways of carrying out the analysis. In the first group, we find models relying strongly on some physical insight, such as the transmission line model [1]–[3], a geometrical theory of reflection [4], and the cavity model [5]–[7]. These techniques yield fairly good results, but are inherently limited to simple shapes even if some generalizations are possible [8], [9]. Edge and feed effects are included in an approximate way and the errors so introduced are difficult to estimate.

In the second group, we have numerical techniques such as segmentation [10], full-wave analysis [11], and methods based on exact computation of the Green function [12]–[14]. The segmentation model is well suited to arbitrary shapes but still cannot take the edge effects precisely into account. Full-wave analysis, although rigorous, appears limited to simple shapes because of lengthy computing times. The Green function approach can handle almost any shape of patch resonator. However, unknowns are defined over the entire surface of the patch, often leading to prohibitively large computing times.

In the CAD context, we need both accurate and computer-efficient models able to analyze arbitrarily shaped patch resonators with various feed mechanisms. Here, we propose such a model based on a generalized edge boundary condition (GEBC). The unknowns are defined along the edge of the structure only and thus the method can be considered one-dimensional. This crucial feature is the main reason behind the numerical efficiency.

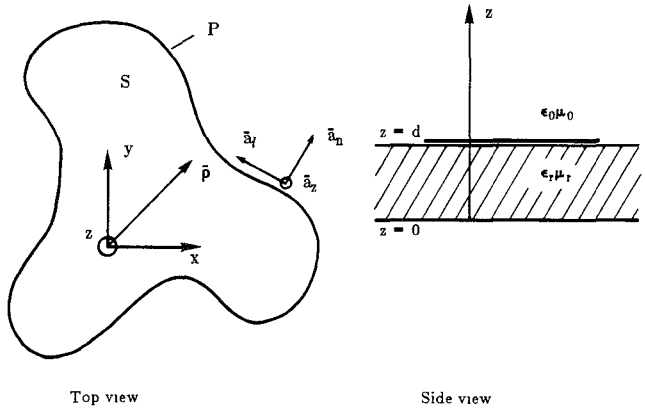

Fig. 1. Arbitrarily shaped microstrip patch resonator.

We will start by describing the model used for the arbitrarily shaped patch. Second, we analyze the probe-fed patch in detail and the technique is then adapted to the simpler case of the strip-fed resonator. Some comments are also given on how to include losses. Finally, the present theory is checked against previously published measured results. The time convention $e^{t\omega t}$ is used throughout.

II. Description of the Patch

Consider an arbitrarily shaped microstrip patch resonator as shown in Fig. 1. A local coordinate system $(\bar{a}_n, \bar{a}_l, \bar{a}_z)$ is defined everywhere along the edge. The dielectric substrate (ϵ_r, μ_r) of thickness d is considered electrically thin $(k_0 d(\epsilon_r\mu_r)^{1/2} \ll 1)$ such that only the dominant TEM mode can propagate in the corresponding parallel-plate waveguide. At each point along the edge, we define an equivalent voltage $V(l)$ and an equivalent current $I(l)$ as follows:

$$V(l) = -dE_z^{\mathrm{TEM}}(l) \tag{1}$$

$$I(l) = H_l^{\mathrm{TEM}}(l). \tag{2}$$

A generalized boundary condition in integral form relates these two quantities everywhere along the edge of the structure, taking care of the dynamical edge effects and the

Manuscript received April 28, 1987; revised October 16, 1987. This work was supported in part by the U.S. Office of Naval Research under Contract N00014-86-K-0417.

The authors are with the Department of Electrical and Computer Engineering, University of Colorado, Boulder, CO 80309.

IEEE Log Number 8718676.

0018-9480/88/0200-0324$01.00 ©1988 IEEE

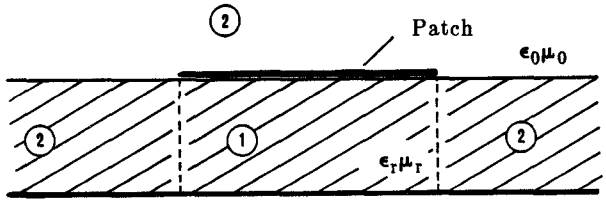

1 - Interior region

2 - Exterior region

Fig. 2. Interior and exterior regions.

mutual coupling between different edge points [15], [16]:

$$I(l)=\frac{i\omega\epsilon_0}{\pi}\left\{-F(\epsilon_r)V(l)+\frac{1}{2}\oint_P V(l')[\bar{a}_l'\cdot\bar{a}_l]G_d(l,l')\,dl'\right\}+\frac{i}{\pi\omega\mu_0}\left\{-\frac{\partial^2V(l)}{\partial l^2}F\left(\frac{1}{\mu_r}\right)+\frac{1}{2}\frac{\partial}{\partial l}\oint_P\frac{\partial V}{\partial l'}G_d(l,l')\,dl'\right\} \tag{3}$$

where P is the perimeter of the patch,

$$G_d(l,l')=\frac{e^{-ik_0(|\bar{\rho}-\bar{\rho}'|^2+d^2)^{1/2}}}{(|\bar{\rho}-\bar{\rho}'|^2+d^2)^{1/2}}\qquad[\bar{\rho},\bar{\rho}'\in P]$$

and

$$F(x)=\ln 2+2xQ_0\left[\frac{1-x}{1+x}\right]-x\ln(2\pi)-1$$

$$Q_0(x)=\sum_{m=1}^{\infty}x^m\ln m$$

$$k_0=\omega(\epsilon_0\mu_0)^{1/2}.$$

This GEBC comes from an integral relation solved with the assumption that the substrate is electrically thin ($kd \ll 1$). Comparisons with experimental results have shown that this GEBC gives accurate results for patches at least as thick as $kd=0.2$. Thicker substrates bring new challenges, not limited to the present approach, such as difficulties in modeling feed effects.

We can see the patch as the juxtaposition of two regions, as shown in Fig. 2. The first, called the interior region, is the dielectric volume bounded by the edge of the structure. The second, called the exterior region, consists of the entire space outside of the patch, the edge playing the role of an interface between the two regions.

For the circuit designer, the input impedance of the structure at various frequencies and in particular close to resonance is the most important parameter to solve for. The critical step in achieving this goal requires finding the equivalent edge voltage. In order to carry out a numerical solution, we must first discretize the arbitrarily shaped patch's edge into a collection of N segments, as shown in Fig. 3. The segments, not necessarily of equal length, should model the patch as closely as possible. If we

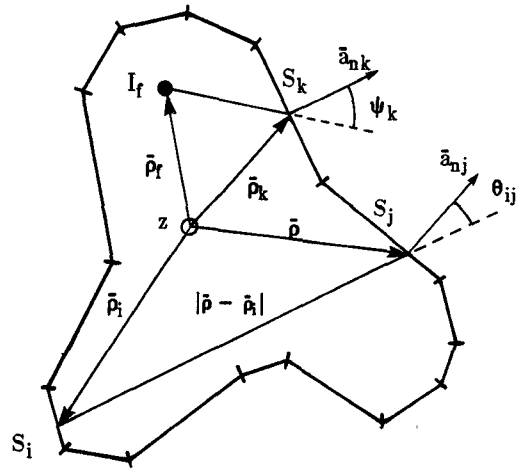

Fig. 3. Segmentation of the probe-fed patch.

consider a strip-fed resonator, a suitable portion of the feed line must be included to take care of the junction effects. Equivalent edge voltages and currents are replaced along a given segment by the middle-point values. As a result, we have an N-port interface connecting the interior region and exterior region networks.

III. Probe-Fed Patch: The Interior Network

Consider the Green function G satisfying the two-dimensional wave equation in the parallel-plate region:

$$(\nabla_t^2+k^2)G(\bar{\rho},\bar{\rho}')=-\delta(\bar{\rho}-\bar{\rho}') \tag{4}$$

where ∇_t is the transverse operator $\partial_x\bar{a}_x+\partial_y\bar{a}_y$; k is the wavenumber in the dielectric, $k=k_0(\epsilon_r\mu_r)^{1/2}$; and $\bar{\rho}=x\bar{a}_x+y\bar{a}_y$. It is well known that the solution of (4) is given by

$$G(\bar{\rho},\bar{\rho}')=-\frac{i}{4}\boldsymbol{H}_0^{(2)}(k|\bar{\rho}-\bar{\rho}'|) \tag{5}$$

where $\boldsymbol{H}_0^{(2)}$ is the Hankel function of the second kind of order 0. The z-directed electric field $E_z\bar{a}_z$ satisfies the wave equation in the dielectric:

$$(\nabla_t^2+k^2)E_z=i\omega\mu_0\mu_rJ_z \tag{6}$$

where J_z is a z-directed and z-independent current source. Assuming uniform current distribution around the circumference of the probe, the current in the feed can be considered as a line source:

$$J_z=I_f\delta(\bar{\rho}-\bar{\rho}_f) \tag{7}$$

where $\bar{\rho}_f$ is the location of the center of the probe. Recall Green's theorem:

$$\oint_S(G\nabla_t^2E_z-E_z\nabla_t^2G)\,ds=\oint_P\left(G\frac{\partial E_z}{\partial n}-E_z\frac{\partial G}{\partial n}\right)dl \tag{8}$$

where S is the surface and P the perimeter of the patch. We now combine (4)–(7) into (8) in a customary way to

find the electrical field at an interior point:

$$E_z(\bar{\rho}') = -\frac{\omega\mu_0\mu_r}{4} I_f \boldsymbol{H}_0^{(2)}(k|\bar{\rho}_f - \bar{\rho}'|) + \frac{1}{4i}\oint_P dl \left[\boldsymbol{H}_0^{(2)}(k|\bar{\rho} - \bar{\rho}'|)\frac{\partial E_z}{\partial n} - \frac{\partial\left[\boldsymbol{H}_0^{(2)}(k|\bar{\rho} - \bar{\rho}'|)\right]}{\partial n} E_z\right] \tag{9}$$

with $\bar{\rho} \in P$ and $\bar{\rho}' \notin P$.

As $\bar{\rho}'$ approaches the edge of the patch, we need a careful evaluation, very similar to the one found in [17]. We find, after a limiting process [18],

$$E_z(\bar{\rho}') = -\frac{\omega\mu_0\mu_r}{2} I_f \boldsymbol{H}_0^{(2)}(k|\bar{\rho}_f - \bar{\rho}'|) + \frac{1}{2i}\oint_P dl \left[\boldsymbol{H}_0^{(2)}(k|\bar{\rho} - \bar{\rho}'|)\frac{\partial E_z}{\partial n} - \frac{\partial\left[\boldsymbol{H}_0^{(2)}(k|\bar{\rho} - \bar{\rho}'|)\right]}{\partial n} E_z\right] \tag{10}$$

where now both $\bar{\rho}$ and $\bar{\rho}'$ belong to the perimeter P.

Considering a locally straight edge, we can apply Faraday's equation to relate the normal derivative of the z-directed electric field to the tangential component of the magnetic field at the edge:

$$\partial_n E_z = i\omega\mu_0\mu_r H_l. \tag{11}$$

Also, from geometrical considerations,

$$\frac{\partial\left[\boldsymbol{H}_0^{(2)}(k|\bar{\rho} - \bar{\rho}'|)\right]}{\partial n} = -k\cos\theta \boldsymbol{H}_1^{(2)}(k|\bar{\rho} - \bar{\rho}'|) \tag{12}$$

where θ is the angle defined between $(\bar{\rho} - \bar{\rho}')$ and $\bar{a}_n(\bar{\rho})$. Directly from the above two equations and the equivalences between field and circuit quantities (1) and (2), we can rewrite (10) as

$$V(l') = \frac{\omega\mu_0\mu_r d}{2} I_f \boldsymbol{H}_0^{(2)}(k|\bar{\rho}_f - \bar{\rho}'|) - \frac{1}{2}\oint_P dl \left[\omega\mu_0\mu_r d\boldsymbol{H}_0^{(2)}(k|\bar{\rho} - \bar{\rho}'|)I(l) + ik\cos\theta \boldsymbol{H}_1^{(2)}(k|(\bar{\rho} - \bar{\rho}'|)V(l)\right]. \tag{13}$$

Introducing the discretization of the patch shown in Fig. 3,

$$V(l_i) = \frac{\omega\mu_0\mu_r d}{2} I_f \boldsymbol{H}_0^{(2)}(k|\bar{\rho}_f - \bar{\rho}_i|) - \frac{\omega\mu_0\mu_r d}{2}\sum_{j=1}^{N}\int_{S_j} dl \boldsymbol{H}_0^{(2)}(k|\bar{\rho} - \bar{\rho}_i|)I(l_j) - \frac{ik}{2}\sum_{\substack{j=1\\ j\neq i}}^{N}\int_{S_j} dl\cos\theta_{ij}\boldsymbol{H}_1^{(2)}(k|\bar{\rho} - \bar{\rho}_i|)V(l_j) \tag{14}$$

where l_i is the edge coordinate of the middle point of segment S_i, $\bar{\rho}_i$ is the vector coordinate of the same point, and θ_{ij} is the angle between $(\bar{\rho} - \bar{\rho}_i)$ and $\bar{a}_{nj}$, the unit vector perpendicular to the segment S_j, as shown in Fig. 3. The relation (14) can be put in the following matrix form:

$$[U][V] = [V_f] + [B][I] \tag{15}$$

where $[V]$ and $[I]$ are unknown column matrices, $[V_f]$ is the source column matrix, and $[U]$ and $[B]$ are square matrices.

IV. Probe-Fed Patch: The Exterior Network

We will use the same contour discretization for the exterior problem as for the interior one. Thus, we can rewrite the GEBC (3) with the help of (1) and (2) as

$$I(l_i) = \frac{i\omega\epsilon_0}{2\pi\Delta_i}\sum_{j=1}^{N} V(l_j)\left[\bar{a}_{li}\cdot\bar{a}_{lj}\right] \cdot\int_{S_j} dl'\int_{S_i} dl \frac{e^{-ik_0(|\bar{\rho}-\bar{\rho}'|^2+d^2)^{1/2}}}{\left(|\bar{\rho}-\bar{\rho}'|^2+d^2\right)^{1/2}} - \frac{i\omega\epsilon_0}{\pi}V(l_i)F(\epsilon_r) - \frac{i}{\pi\omega\mu_0}\left.\frac{\partial^2 V(l)}{\partial l^2}\right|_{l=l_i} \cdot F\left(\frac{1}{\mu_r}\right) + \frac{i}{2\pi\omega\mu_0\Delta_i}\cdot\sum_{j=1}^{N}\left.\frac{\partial V(l)}{\partial l}\right|_{l=l_j}\int_{S_j} dl' \cdot\left\{\frac{e^{-ik_0(|\bar{e}_i-\bar{\rho}'|^2+d^2)^{1/2}}}{\left(|\bar{e}_i-\bar{\rho}'|^2+d^2\right)^{1/2}} - \frac{e^{-ik_0(|\bar{e}_{i-1}-\bar{\rho}'|^2+d^2)^{1/2}}}{\left(|\bar{e}_{i-1}-\bar{\rho}'|^2+d^2\right)^{1/2}}\right\} \tag{16}$$

where Δ_i is the length of the segment S_i, $\bar{a}_{li}$ is the unit vector tangent to the segment S_i, and $\bar{e}_i = \bar{\rho}_i + \bar{a}_{li}\Delta_i/2$. In this context, we found that a finite difference evaluation of the edge derivatives was accurate enough. Defining $h_i = (\Delta_i + \Delta_{i-1})/2$, we have

$$\left.\frac{\partial V}{\partial l}\right|_{l=l_i} = \frac{h_i^2 V_{i+1} - h_{i+1}^2 V_{i-1} + \left(h_{i+1}^2 - h_i^2\right)V_i}{h_i h_{i+1}(h_i + h_{i+1})} + O(h^2)$$

$$\left.\frac{\partial^2 V}{\partial l^2}\right|_{l=l_i} = \frac{2\left[h_i V_{i+1} + h_{i+1}V_{i-1} - (h_i + h_{i+1})V_i\right]}{h_i h_{i+1}(h_i + h_{i+1})} + O(h) \tag{17}$$

where V_i is a shorthand notation for $V(l_i)$. After some reorganization of the terms and incorporating the two

above relations, (16) becomes

$$
\begin{aligned}
I(l_i) = &\left[\frac{i\omega\epsilon_0}{\pi\Delta_i} \int_0^{\Delta_i} dx \, \frac{(\Delta_i - x) e^{-ik_0(x^2+d^2)^{1/2}} - \Delta_i}{(x^2+d^2)^{1/2}} \right. \\
&\left. + \frac{i\omega\epsilon_0}{\pi} \sinh^{-1}\left[\frac{\Delta_i}{d}\right] - \frac{i\omega\epsilon_0}{\pi} F(\epsilon_r) + \frac{2iF\left(\frac{1}{\mu_r}\right)}{\pi\omega\mu_0 h_i h_{i+1}} \right] V(l_i) \\
&- \left[\frac{2iF\left(\frac{1}{\mu_r}\right)}{\pi\omega\mu_0 h_i (h_i + h_{i+1})} \right] V(l_{i-1}) \\
&- \left[\frac{2iF\left(\frac{1}{\mu_r}\right)}{\pi\omega\mu_0 h_{i+1} (h_i + h_{i+1})} \right] V(l_{i+1}) \\
&+ \left[\sum_{\substack{j=1 \\ j\neq i}}^{N} \frac{i\omega\epsilon_0 [\bar{a}_{li} \cdot \bar{a}_{lj}]}{2\pi\Delta_i} \int_{S_i} dl \int_{S_j} dl' \frac{e^{-ik_0(|\bar{\rho}-\bar{\rho}'|^2+d^2)^{1/2}}}{(|\bar{\rho}-\bar{\rho}'|^2+d^2)^{1/2}} \right. \\
&+ \sum_{\substack{j=1 \\ j\neq i}}^{N} \frac{i(h_{j+1}-h_j)}{2\pi\omega\mu_0\Delta_i h_j h_{j+1}} \int_{S_j} dl' \\
&\cdot \left\{ \frac{e^{-ik_0(E_i^2+d^2)^{1/2}}}{(E_i^2+d^2)^{1/2}} - \frac{e^{-ik_0(F_i^2+d^2)^{1/2}}}{(F_i^2+d^2)^{1/2}} \right\} \\
&+ \sum_{\substack{j=1 \\ j\neq i-1}}^{N} \frac{-ih_{j+2}}{2\pi\omega\mu_0\Delta_i h_{j+1}(h_{j+1}+h_{j+2})} \int_{S_{j+1}} dl' \\
&\cdot \left\{ \frac{e^{-ik_0(E_i^2+d^2)^{1/2}}}{(E_i^2+d^2)^{1/2}} - \frac{e^{-ik_0(F_i^2+d^2)^{1/2}}}{(F_i^2+d^2)^{1/2}} \right\} \\
&+ \sum_{\substack{j=1 \\ j\neq i+1}}^{N} \frac{ih_{j-1}}{2\pi\omega\mu_0\Delta_i h_j (h_{j-1}+h_j)} \int_{S_{j-1}} dl' \\
&\left. \cdot \left\{ \frac{e^{-ik_0(E_i^2+d^2)^{1/2}}}{(E_i^2+d^2)^{1/2}} - \frac{e^{-ik_0(F_i^2+d^2)^{1/2}}}{(F_i^2+d^2)^{1/2}} \right\} \right] V(l_j)
\end{aligned}
\tag{18}
$$

where

$$
E_i^2 = |\bar{e}_i - \bar{\rho}'|^2
$$

$$
F_i^2 = |\bar{e}_{i-1} - \bar{\rho}'|^2.
$$

We can immediately put (18) into a matrix form:

$$
[I] = [S][V] \tag{19}
$$

where $[I]$ and $[V]$ are the same unknown column vectors as in (15) and $[S]$ is a square matrix.

V. Probe-Fed Patch: The Input Impedance

The incident electric field E_z^{inc} is given by the solution of the wave equation (6) in an unbounded parallel plate region:

$$
E_z^{\text{inc}} = -\frac{\omega\mu_0\mu_r I_f}{4} \boldsymbol{H}_0^{(2)}(k|\bar{\rho} - \bar{\rho}_f|).
$$

The tangential electric field produced by I_f on the surface of the probe of radius a is given by

$$
E_z^{\text{inc}}\big|_{|\bar{\rho}-\bar{\rho}_f|=a} = -\frac{\omega\mu_0\mu_r I_f}{4} \boldsymbol{H}_0^{(2)}(ka). \tag{20}
$$

In order to compute the input impedance, we must find the tangential electric field on the surface of the probe. We can consider this electric field as the sum of two terms, namely an incident and a scattered field. The incident term corresponds to the field produced by I_f in an infinite parallel-plate region, evaluated at the surface of the probe. The scattered term corresponds to the field "reflected" off the boundary. As far as the scattered field is concerned, we can approximate its value on the surface of the probe by its value at the center of the feed $\bar{\rho} = \bar{\rho}_f$. Directly from (9), with the source term removed,

$$
E_z^s(\bar{\rho}_f) = \frac{1}{4i} \oint_P dl \left[\boldsymbol{H}_0^{(2)}(k|\bar{\rho} - \bar{\rho}_f|) \frac{\partial E_z}{\partial n} - \frac{\partial \left[\boldsymbol{H}_0^{(2)}(k|\bar{\rho} - \bar{\rho}_f|) \right]}{\partial n} E_z \right].
$$

Replacing the field quantities by their equivalent circuit counterparts (1) and (2), we can rewrite the above equation as

$$
E_z^s(\bar{\rho}_f) = \frac{1}{4i} \oint_P dl \left[i\omega\mu_0\mu_r \boldsymbol{H}_0^{(2)}(k|\bar{\rho} - \bar{\rho}_f|) I(l) - \frac{k\cos\psi}{d} \boldsymbol{H}_1^{(2)}(k|\bar{\rho} - \bar{\rho}_f|) V(l) \right] \tag{21}
$$

where ψ is the angle between $(\bar{\rho} - \bar{\rho}_f)$ and $\bar{a}_n(\bar{\rho})$. The input impedance is given by the following expression [19]:

$$
Z_{\text{in}} = -\frac{E_z\big|_{|\bar{\rho}-\bar{\rho}_f|=a} d}{I_f}. \tag{22}
$$

Therefore, based on (21) and (22), the input impedance can be expressed as a contour integral:

$$
Z_{\text{in}} = \frac{\omega\mu_0\mu_r d}{4} \boldsymbol{H}_0^{(2)}(ka) - \frac{\omega\mu_0\mu_r d}{4I_f} \oint_P dl \, \boldsymbol{H}_0^{(2)}(k|\bar{\rho} - \bar{\rho}_f|) I(l) + \frac{k}{4iI_f} \oint_P dl \cos\psi \boldsymbol{H}_1^{(2)}(k|\bar{\rho} - \bar{\rho}_f|) V(l).
$$

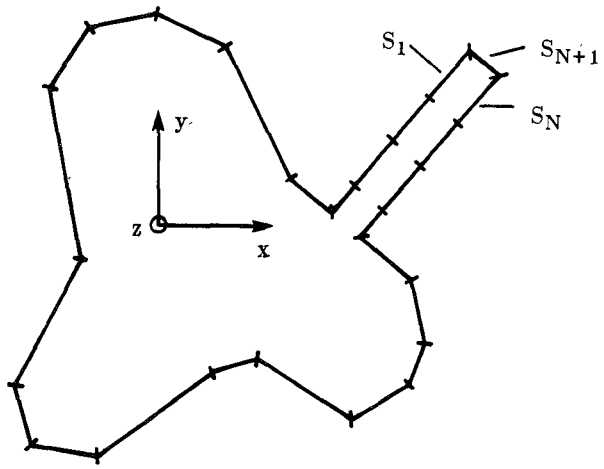

Fig. 4. Segmentation of the strip-fed patch.

Discretizing the contour, we can approximate the above equation:

$$Z_{\text{in}} = \frac{\omega\mu_0\mu_r d}{4} H_0^{(2)}(ka) - \frac{\omega\mu_0\mu_r d}{4I_f} \sum_{k=1}^{N} H_0^{(2)}(k|\bar{\rho}_k - \bar{\rho}_f|)\Delta_k I(l_k) - \frac{ik}{4I_f} \sum_{k=1}^{N} \cos\psi_k H_1^{(2)}(k|\bar{\rho}_k - \bar{\rho}_f|)\Delta_k V(l_k) \quad (23)$$

where ψ_k is the angle between $(\bar{\rho}_k - \bar{\rho}_f)$ and $\bar{a}_{nk}$. The input impedance Z_{in} can thus be easily computed once we have solved for the edge voltages $V(l_k)$ and currents $I(l_k)$. Often, an interpolation of the edge voltages and current proves helpful when the feed is located near the edge of the patch. Directly based on the matrix equations (15) and (19), we can solve for the unknown edge voltages:

$$\{[U]-[B][S]\}[V] = [V_f] \quad (24)$$

and (19) thereafter yields the edge currents. We can then compute the input impedance Z_{in} as given by (23).

VI. Strip-Fed Patch

The treatment of the strip-fed patch resonator follows closely the approach used for the probe-fed patch. One of the principal difficulties of earlier CAD models has been to include the feed junction effects. Here, we solve this difficulty by including a suitable portion of the feed in the patch discretization. A feed length of $\lambda_0/16$ is sufficient in most cases. The feeding strip is then truncated and an additional $(N+1)$th segment is placed at the truncation, as shown in Fig. 4.

Since the source term under the patch is absent, the interior problem can be written in matrix form as

$$[U][V]+[U']V(l_{N+1}) = [B][I]+[B']I(l_{N+1}) \quad (25)$$

where we have segregated the quantities pertaining to the $(N+1)$th port. $[U]$ and $[B]$ are rectangular matrices with $(N+1)$ rows and N columns, $[U']$ and $[B']$ are column vectors of dimension $(N+1)$, and $[V]$ and $[I]$ are unknown column vectors of dimension N. The exterior matrix formulation is still given by (19) with $[S]$ a square matrix of dimension N. Without loss of generality, we can normalize the input current at the $(N+1)$th port to unity. Therefore, the matrix equation to solve for $V(l_{N+1})$ can be written as

$$\{[U]-[B][S]\}[V]+[U']V(l_{N+1}) = [B']. \quad (26)$$

Once this input voltage is obtained, the input impedance Z_{in} follows directly:

$$Z_{\text{in}} = -\frac{V(l_{N+1})}{\Delta_{N+1}}. \quad (27)$$

VII. Dielectric and Conductor Losses

Although losses are rather small in most applications, they still produce a noticeable effect on the real part of the input impedance. A correct estimate of the losses is thus important. We can easily take care of dielectric losses by introducing a complex component of the permittivity. On the other hand, conduction losses are more difficult to evaluate. We have found a simple and satisfactory approach to include this effect based on an equivalent permeability of the substrate.

The basic idea is to recall well-known cavity perturbation expressions for the frequency shift in a cavity in terms of wall losses and magnetic losses [20]. As far as losses are concerned, it is probably accurate enough to treat the patch resonator as a cavity. Since the TEM field has no z variation, we can easily relate surface and volume integrals. The frequency shift due to wall losses is given by

$$\frac{\omega-\omega_0}{\omega} \approx \frac{(1-i)}{\omega d} \frac{\int_V \left(\frac{\omega\mu_0}{2\sigma}\right)^{1/2} \bar{H}\cdot\bar{H}_0\, dV}{\int_V [\epsilon_0\epsilon_r \bar{E}\cdot\bar{E}_0 - \mu_0\mu_r \bar{H}\cdot\bar{H}_0]\, dV}$$

where the subscript 0 identifies unperturbed quantities. Similarly, the frequency shift due to a perturbation $\Delta\mu$ is

$$\frac{\omega-\omega_0}{\omega} \approx \frac{\int_V \Delta\mu \bar{H}\cdot\bar{H}_0\, dV}{\int_V [\epsilon_0\epsilon_r \bar{E}\cdot\bar{E}_0 - \mu_0\mu_r \bar{H}\cdot\bar{H}_0]\, dV}.$$

We can thus relate conductor losses to an equivalent change in permeability:

$$\Delta\mu = \frac{1}{d}\left(\frac{\mu_0}{2\omega}\right)^{1/2}\left[\frac{1}{\sqrt{\sigma_t}} + \frac{1}{\sqrt{\sigma_b}}\right](1-i) \quad (28)$$

where σ_t and σ_b are the conductivity of the top patch and ground plane, respectively.

VIII. Comparison with Experimental Results

In order to check our theoretical results, we have made several comparisons with previously published measured results. In all cases where detailed information on the experimental procedure was given, we were consistently able to get good agreement. Here we present the results for

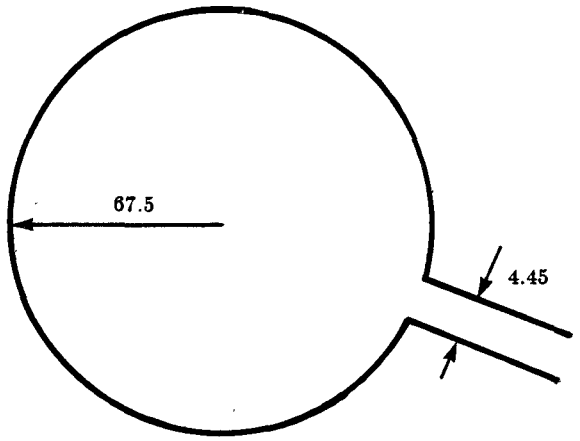

Fig. 5. Circular strip-fed patch. (Dimensions in mm). $\epsilon_r = 2.62$, $\tan\delta = 0.001$, $\sigma_t = \sigma_b = 2.9 \cdot 10^7$, $d = 1.59$ mm, feed length = 3.0 cm, 84 segments.

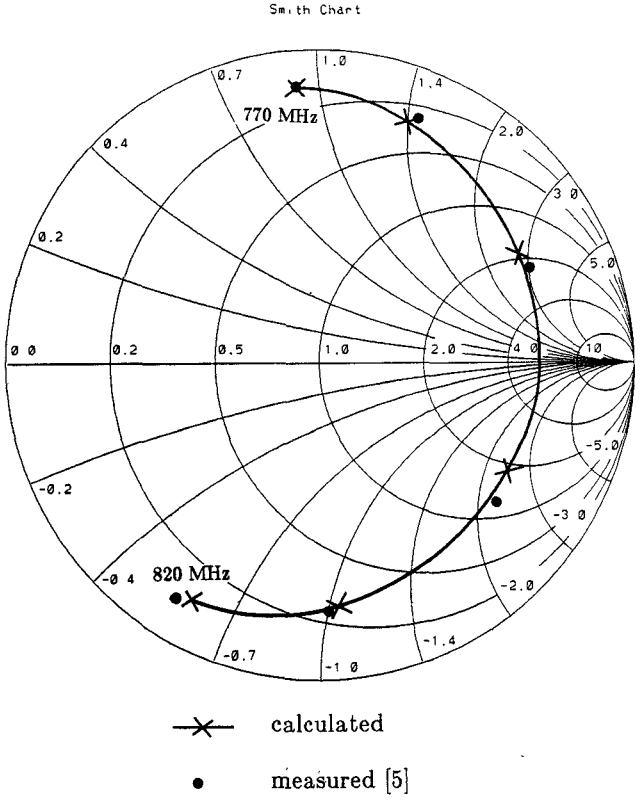

Fig. 6. Input impedance of the circular patch. (Reference plane at the junction, 10 MHz increment.)

three different microstrip patch resonators. As a first example, we have taken the strip-fed circular patch, shown in Fig. 5. In Fig. 6, we see a good match with the measured input impedance [5]. The strip-fed triangular patch, shown in Fig. 7, gives a second comparison (Fig. 8). Finally, the third example deals with the folded dipole resonator shown in Fig. 9. This probe-fed patch provides a critical test of our approach due to the multiplicity of edge interactions and the proximity between the feed and the edge. In this example, we have chosen to look at the third resonance so as to have an electrically thicker substrate. Here again, we have good agreement with experimental results [21], as shown in Fig. 10. A few comments will help in interpreting

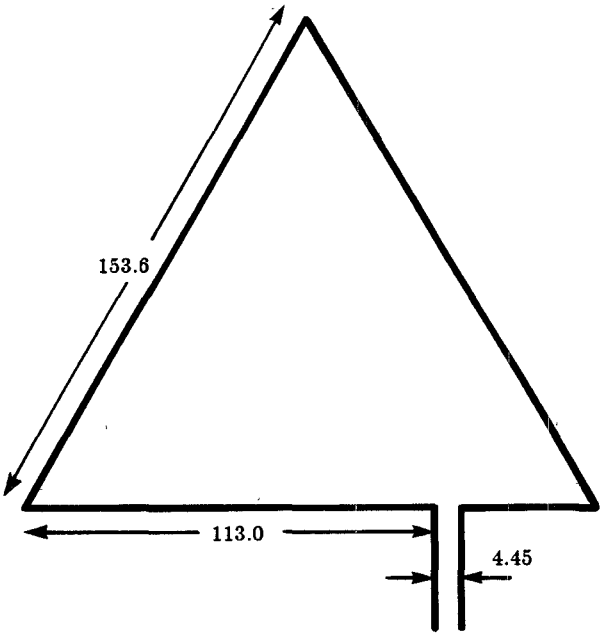

Fig. 7. Equilateral triangular strip-fed patch (dimensions in mm). $\epsilon_r = 2.62$, $\tan\delta = 0.001$, $\sigma_t = \sigma_b = 2.9 \cdot 10^7$, $d = 1.59$ mm, feed length = 3.0 cm, 68 segments.

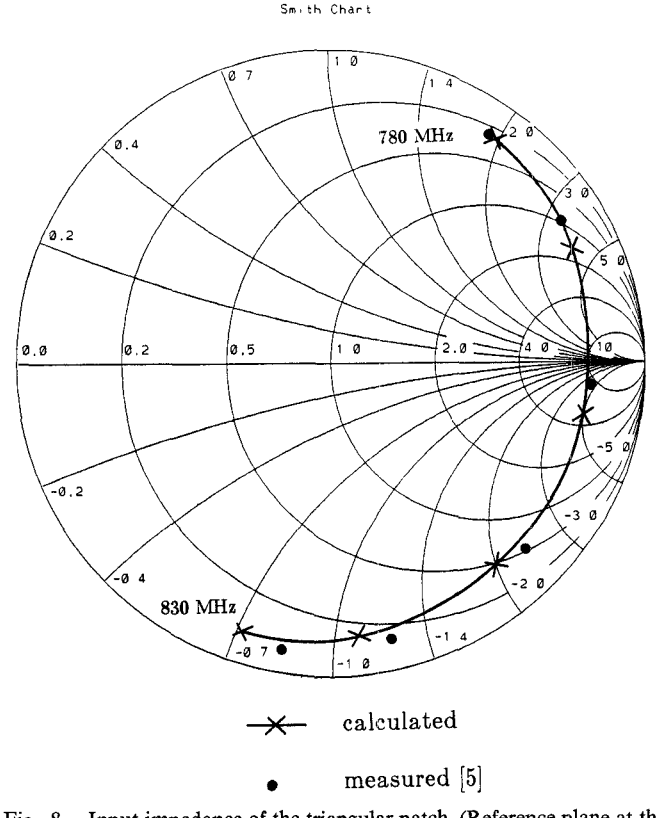

Fig. 8. Input impedance of the triangular patch. (Reference plane at the junction, 10 MHz increment.)

the results:

1) The simplicity of the patch shapes analyzed here has been dictated by the availability of measured results, not the limitations of the theory. Since these results were available on Smith charts, we have kept this representation.

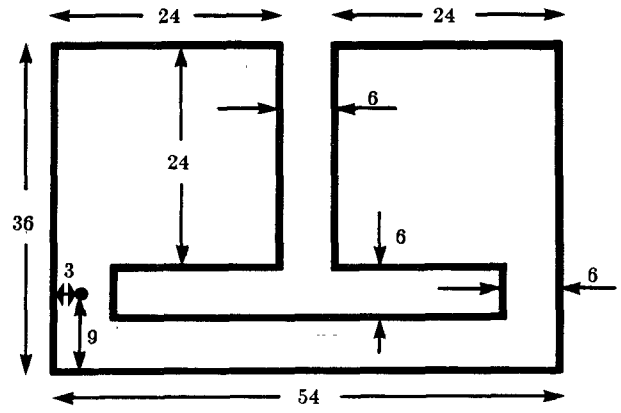

Fig. 9. Probe-fed folded dipole patch (dimensions in mm). $\epsilon_r = 4.34$, $\tan\delta = 0.02$, $\sigma_t = \sigma_b = 2.9 \cdot 10^7$, $d = 0.8$ mm, $a = 0.5$ mm, 128 segments.

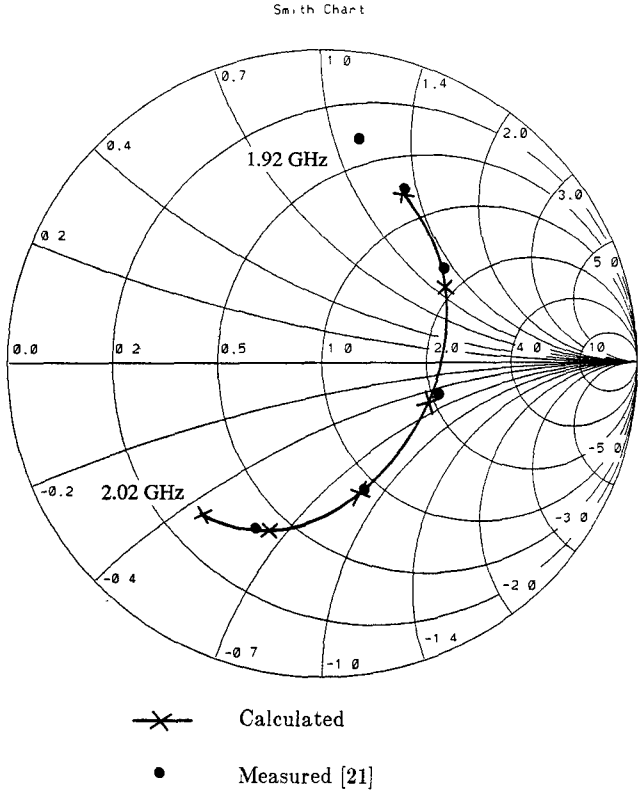

Fig. 10. Input impedance of the folded dipole. (Third resonance, reference at the ground plane, 0.02 GHz increment.)

2) It is probably reasonable to assume at least 0.5 percent experimental uncertainty on the resonant frequency.
3) The influence of surface roughness on the conductivity of the metallic surfaces is difficult to estimate. We have assumed the conductivity to be half that of bulk copper.
4) The method proposed here is numerically efficient. We can see this in two places. First, the elements of the matrices are easily computed. In particular, the numerical integrations require very few function evaluations. Second, for large and complicated structures, the numerical efficiency is directly related to the number of unknowns. Since this is true for most numerical methods, an edge discretization will generally give smaller matrices, and thus lead to shorter computing times.

IX. Conclusions

A new model has been developed to accurately predict the input impedance of arbitrarily shaped microstrip patch resonators. This computer-efficient approach leads to good agreement between theoretical and experimental results for a variety of commonly used patch shapes.

The method is easily adaptable to probe-type and strip-type feeds. Furthermore, the model works always with the actual parameters of the patch. In particular the feed is modeled by its physical dimensions and no edge extensions or equivalent dielectric constant are used. Finally we must point out that the present theory is compatible with other analysis techniques, such as segmentation, which is particularly attractive for CAD applications.

References

[1] R. E. Munson, "Conformal microstrip antennas and microstrip phased arrays," *IEEE Trans. Antennas Propagat.*, vol. AP-22, pp. 74–78, Jan. 1974.
[2] A. G. Derneryd, "Linearly polarized microstrip antennas," *IEEE Trans. Antennas Propagat.*, vol. AP-24, pp. 846–851, Nov. 1976.
[3] H. Pues and A. Van de Capelle, "Accurate transmission-line model for the rectangular microstrip antenna," *Proc. Inst. Elec. Eng.*, pt. H, vol. 131, pp. 334–340, Dec. 1984.
[4] D. C. Chang, "Analytical theory of an unloaded rectangular microstrip patch," *IEEE Trans. Antennas Propagat.*, vol. AP-29, pp. 54–62, Jan. 1981.
[5] Y. T. Lo *et al.*, "Study of microstrip antennas, microstrip phased arrays, and microstrip feed networks," Final Rep. RADC-TR-77-406, under contract AF19628-76-C-0140, Oct. 1977.
[6] W. F. Richards, Y. T. Lo, and D. D. Harrison, "An improved theory for microstrip antennas and applications," *IEEE Trans. Antennas Propagat.*, vol. AP-29, pp. 38–46, Jan. 1981.
[7] K. R. Carver and J. W. Mink, "Microstrip antenna technology," *IEEE Trans. Antennas Propagat.*, vol. AP-29, pp. 2–24, Jan. 1981.
[8] A. K. Bhattacharyya and R. Garg, "Generalized transmission line model for microstrip patches," *Proc. Inst. Elec. Eng.*, pt. H, vol. 132, pp. 93–98, Apr., 1985.
[9] G. Dubost, "Linear transmission-line model analysis of arbitrary-shape patch antennas," *Electron Lett.*, vol. 22, pp. 798–799, July 1986.
[10] K. C. Gupta and P. C. Sharma, "Segmentation and desegmentation techniques for analysis of planar microstrip antennas," in *IEEE Int. Antennas Propagat. Symp. Proc.* (Los Angeles), June 1981, pp. 19–22.
[11] T. Itoh and W. Menzel, "A full-wave analysis method for open microstrip structures," *IEEE Trans. Antennas Propagat.*, vol. AP-29, pp. 63–68, Jan. 1981.
[12] D. M. Pozar, "Input impedance and mutual coupling of rectangular microstrip antennas," *IEEE Trans. Antennas Propagat.*, vol. AP-30, pp. 1191–1196, Nov. 1982.
[13] M. C. Bailey and M. D. Deshpande, "Integral equation formulation of microstrip antennas," *IEEE Trans. Antennas Propagat.*, vol. AP-30, pp. 651–656, July 1982.
[14] J. R. Mosig and F. E. Gardiol, "General integral equation formulation for microstrip antennas and scatterers," *Proc. Inst. Elec. Eng.*, pt. H, vol. 132, pp. 424–432, Dec. 1985.
[15] T. M. Martinson and E. F. Kuester, "Resonant modes and input impedance of arbitrarily shaped microstrip patches on electrically thin substrate," *Conf. Antennas Commun. (Montech '86) Proc.*, (Montreal), Sept. 1986, pp. 100–103.
[16] T. M. Martinson and E. F. Kuester, "A generalized edge boundary condition for open microstrip structures," Scientific Report No. 91, Electromagnetics Laboratory, Department of Electrical and Computer Engineering, University of Colorado, Aug. 1987.

[17] T. Okoshi and T. Miyoshi, "The planar circuit—An approach to microwave integrated circuitry," *IEEE Trans. Microwave Theory Tech.*, vol. MTT-20, pp. 245–252, Apr. 1972.
[18] J. Van Bladel, *Electromagnetic Fields*. Washington: Hemisphere Pub., 1985, pp. 391–393.
[19] J. Venkataraman and D. C. Chang, "Input impedance to a probe-fed rectangular microstrip patch antenna," *Electromagnetics*, vol. 3, pp. 387–399, 1983.
[20] R. F. Harrington, *Time-Harmonic Electromagnetic Fields*. New York: McGraw-Hill, 1961, pp. 371–372.
[21] J. R. Mosig, "Les structures microruban: analyse au moyen des équations intégrales," Doctoral dissertation, Swiss Federal Institute of Technology, Lausanne, Switzerland, 1984, p. 308.

✠

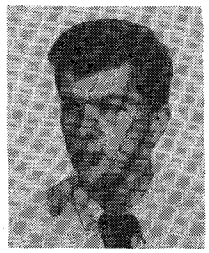

Thomas M. Martinson was born in Zurich, Switzerland, on May 26, 1959. He received the Diploma degree in electrical engineering from the Swiss Federal Institute of Technology, Lausanne, Switzerland, in 1983. He is currently finishing his graduate studies at the University of Colorado, Boulder.

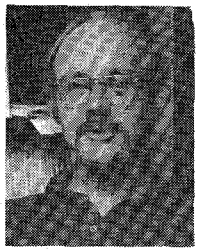

Edward F. Kuester (S'73–M'76) was born in St. Louis, MO, on June 21, 1950. He received the B.S. degree from Michigan State University, East Lansing, in 1971, and the M.S. and Ph.D. degrees from the University of Colorado, Boulder, in 1974 and 1976, respectively, all in electrical engineering.

Since 1976, he has been with the Department of Electrical Engineering at the University of Colorado, Boulder, where he is currently a Professor. In 1979, he was a Summer Faculty Fellow at the Jet Propulsion Laboratory, Pasadena, CA. In 1981–1982, he was a Visiting Professor at the Technische Hogeschool, Delft, The Netherlands. His research interests include the electromagnetic theory of waveguiding and radiating structures at all frequencies, applied mathematics, and applied physics.

Dr. Kuester is a member of the Optical Society of America and Commission B of the International Union of Radio Science.